Materials and Design 198 (2021) 109361

Contents lists available at ScienceDirect

Materials and Design

journal homepage: www.elsevier.com/locate/matdes

Cerium oxide loaded with Gum Arabic as environmentally friendly anti-corrosion additive for protection of coated steel

Muddasir Nawaz [a], R.A. Shakoor [a,*], Ramazan Kahraman [b], M.F. Montemor [c]

[a] Center for Advanced Materials (CAM), Qatar University, 2713 Doha, Qatar
[b] Department of Chemical Engineering, Qatar University, 2713 Doha, Qatar
[c] Centro de Química Estrutural, Departamento de Engenharia Química, Instituto Superior Técnico, Universidade de Lisboa, Av Rovisco Pais, 1049-001 Lisboa, Portugal

HIGHLIGHTS

- Environmentally friendly Anticorrosive pigments (CeO_2 loaded with Gum Arabic) were added in coating for corrosion protection of steel.
- The anti-corrosive pigments were characterized by different techniques and confirmed the loading of Gum Arabic into CeO_2.
- Improved anti-corrosion properties of coated samples were evidenced by Electrochemical Impedance Spectroscopy (EIS) techniques.
- The Corrosion inhibition mechanism suggests that Gum Arabic delays coating degradation and adsorbs on steel substrate to form a protective layer.

GRAPHICAL ABSTRACT

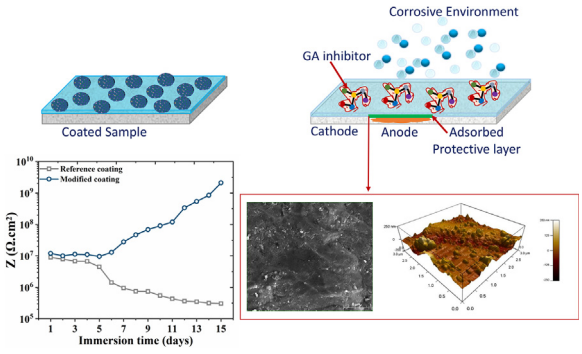

ARTICLE INFO

Article history:
Received 4 August 2020
Received in revised form 17 November 2020
Accepted 23 November 2020
Available online 25 November 2020

Keywords:
Ceria
Coatings
Corrosion inhibition
Steel
Gum Arabic

ABSTRACT

The depreciation of assets and safety threats because of corrosion has forced to develop eco-friendly and smarter corrosion protection strategies. In this study, natural Gum Arabic (GA) was used as a corrosion inhibitor and loaded into cerium oxide nanoparticles (CONPs) to develop an environment-friendly additive for corrosion protection of coated steel in the marine environment. This additive was uniformly dispersed into an epoxy formulation that was used to protect steel plates. Epoxy coatings containing CONPs, without GA, were also prepared as reference. High-Resolution Transmission Electron Microscopy (HR-TEM) and Fourier Transform infrared spectroscopy (FTIR) revealed the successful loading of GA into the CONPs. Thermogravimetric analysis (TGA) and Brunauer-Emmett-Teller (BET) techniques confirmed approximately ~30.0 wt% loading of GA into the CONPs. Electrochemical impedance spectroscopy (EIS) demonstrated the anticorrosion properties of the epoxy coatings modified with the GA loaded CONPs when compared to reference coatings. The corrosion protection mechanism postulates that GA loaded CONPs act as a filler material for epoxy coating and it can also aid the recovery of the protective properties of the epoxy coating leading to the formation of a stable protective layer.

1. Introduction

Corrosion induced degradation of steel structures is one of the most critical issues for a wide range of industries because it leads to severe depreciation of investment and loss in production [1].

* Corresponding author.
E-mail address: shakoor@qu.edu.qa (R.A. Shakoor).

https://doi.org/10.1016/j.matdes.2020.109361

Many types of coatings have been reported in the literature to prevent corrosion of steel components; polymeric coatings have been the most widely used due to their good barrier properties [2–4]. In what concerns polymeric coatings, corrosion protection is due to the coating barrier effect and inhibition of corroding sites [5,6]. The first requires application of thick and impermeable coatings that prevent the contact of the steel material with the corrosive environment [7]; the second involves dispersion of anti-corrosion pigments that inhibit corrosion when the protective barrier effect is lost [8–10]. However, this process is not so simple, since the direct contact of some corrosion inhibitors with the protective matrix may cause unwanted reactions that affect the coating barrier properties negatively. For this reason, the corrosion inhibitors can be loaded into nano/microcarriers with good compatibility with the coating, particularly inorganic ones that may also serve as fillers, enhancing the coating barrier properties. To explore better this process it is important to use carriers that sense specific stimuli and that release the inhibitor when necessary, leading to a smarter corrosion inhibition effect while providing reliable long term corrosion protection [11,12].

In the past, chromate-containing pigments have been widely used as corrosion inhibitors due to their high efficiency and good compatibility with coatings; furthermore, these pigments have been considered the most suitable to impart self-healing ability in coatings. However, the toxicity of chromate-containing pigments has restricted its use, and nowadays it is critical to find alternatives that are more environmentally friendly [13]. In this quest, the interest in renewable and biodegradable corrosion inhibitors has been raised considerably [14,15].

Cerium oxide (CeO_2) has gained significant interest as an additive for polymeric coatings due to some important characteristics such as chemical stability, different morphologies, and structural features and reduced toxicity [16,17]. Although very stable, particularly in alkaline environments, ceria is however able to release cerium ions in acidic conditions as the ones created when anodic dissolution of steel takes place [18]. These cerium ions can then react with hydroxyl anions forming protective hydroxides that have been widely reported as cathodic corrosion inhibitors. Therefore, ceria particles can also have an important role in inhibiting corrosion [19]. Moreover, dispersion of CeO_2 nanoparticles in various paints has led to enhanced corrosion protection due to the formation of an ultrafine network [20] with decreased porosity, and CeO_2 can also serve as carrier for the loading of corrosion inhibitors due to its chemical (and sometimes porous) nature [21].

Naturally occurring inhibitors have emerged as an eco-friendly option and widely considered for protection of different metals and alloys [22,23]. Amongst these, Gum Arabic - GA, which has been used in biological applications because of its good biodegradability and renewable origin has attracted some attention [24]. Gum Arabic serves as film building agent and forms stable protective layers onto metallic substrates either by a reaction with the metal or by the interaction of their surface charges with the dipole charges on the metallic surface [25]. GA has been reported as a green corrosion inhibitor for mild steel in acidic media [26–28], but its loading into carriers to develop smarter anti-corrosion additives for polymeric coating used for corrosion protection of steel in the marine environments has never been reported at author's best knowledge. Thus, this study aims at studying a new anti-corrosion pigment composed of cerium oxide nanoparticles (CONPs) serving as carriers for Gum Arabic (GA) acting as an eco-friendly corrosion inhibitor. The CONPs loaded with GA were uniformly dispersed into an epoxy formulation that was used to coat steel plates. The results demonstrated that the presence of CONPs loaded with GA improved the corrosion resistance of epoxy coated steel coupons. A plausible mechanism to explain such behavior is also discussed.

2. Experimental

2.1. Materials

Cerium oxide nanoparticles (CONPs), sodium hydroxide, and ethanol were purchased from Sigma Aldrich while Gum Arabic (GA) was purchased from Alfa Aesar. Epoxy resin (EPON RESIN 815C) and the curing agent (EPIKURE) was obtained from Hexion chemicals. Plain carbon steel plates (30x30x1 mm^3) having composition (Fe = 99.18%, C = 0.21%, Cu = 0.20%, Mn = 0.30%, P = 0.04%, S = 0.04%) were provided by a local supplier. The steel coupons were cleaned with silicon carbide emery papers (SiC) from 120 to 800 grit purchased from a local source.

2.2. Loading of CeO_2 with Gum Arabic

Dried CONPs in a concentration of 3.0 wt% (relative to the weight of the solution) were soaked into a 10.0 g/L GA water solution and sonicated for 30.0 min. After that, the suspension was dried at 70 °C in the oven for 24 h to remove the excess solvent and the dried CONPs loaded with GA were then placed in the tightly loaded closed container to avoid any contamination. The schematic diagram of the experimental procedure is shown in Fig. 1.

2.3. Preparation of the polymeric coatings on steel substrates

1 wt% of CONPs loaded with GA were 1st thoroughly mixed in the harder, which has less viscosity as compared to epoxy, and thus a homogeneous distribution of nanoparticles was achieved without any agglomeration. After that, it was added into epoxy, followed by ultrasonication for 10 min. The ultrasonication treatment resulted in the proper dispersion of nanoparticles in the epoxy matrix. The stoichiometric ratio of epoxy and hardener was kept (100:25) at room temperature. The epoxy mixture was then coated onto polished steel substrates by a doctor blade to get a uniform thickness of ~150 ± 5 μm. The coated panels were kept for curing at room temperature for 48 h. A set of reference coatings was also prepared by modifying the epoxy monomer with CONPs without GA.

2.4. Characterization of particles and coated samples

The structural and phase purity of CONPs without and with GA were studied by X-ray diffraction (XRD) using a PAN analytical X'pert Pro Cu (Kα), with a scanning rate of 2°/min and scanning angle ranging between $10° \le 2\theta \le 90°$.

The morphological features of the CONPs loaded with GA and modified coatings were studied with a field emission scanning electron microscopy (FE-SEM-Nova Nano-450, Netherland) and High-Resolution Transmission electron microscope HR-TEM TALOS F200X (FEI, New York, NY, USA). Elemental mapping was performed by EDS coupled to the SEM apparatus. FTIR analysis was performed to investigate the change in bonding and the interaction of the loaded CONPs with GA. The spectra were recorded in the range of 4000–500 cm^{-1} in the transmission mode using the FTIR Frontier (PerkinElmer, Frontier, USA). Thermal stability of coatings and CONPs loaded with GA was studied from room temperature up to 600 °C, employing a heating rate of 10 °C/min. TGA and DTA profiles were obtained by the synchronization analyzer (PerkinElmer, TGA 4000, USA). The coating thickness gauge meter (PosiTector 6000) from DeFelsko (Made in USA) was used to measure the thickness of coating samples. The specific surface area and pore volume of CONPs were studied using Brunauer-Emmett-Teller (BET) technique through equipment AimSizer (AS-3012). The charge of CONPs before and after loading of GA was determined through a zeta potential measuring equipment (Malvern, Zeta sizer, Nano ZSP, USA).

Electrochemical impedance measurements were performed to evaluate the corrosion resistance of coated samples for 15 days of

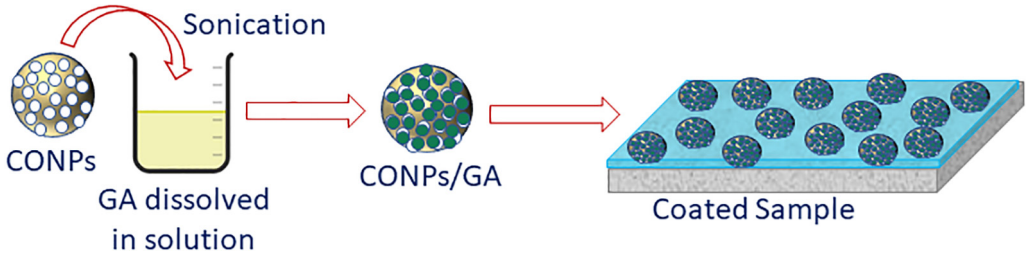

Fig. 1. Schematic diagram of loading of inhibitor and epoxy coating.

immersion in 3.5 wt% NaCl solution at room temperature in the frequency range of 100 kHz to 10 mHz. The Gamry 3000 (30K BOOSTER potentiostat/galvanostate/ZRA, USA) equipment was used for EIS analysis. The EIS measurements were conducted at scan frequency rate of 10 points per decade with an open circuit potential (OCP) for 1 h and the rms signal was varied between 2 and 10 mV.

d.c. potentiodynamic polarization experiments were carried out to investigate the corrosion activity of steel substrates in the presence and absence of GA. Experiments were carried out in 0.1 M NaCl solution after addition of GA in the concentration of 1.00 g/L The polarization measurements were performed in the potential range of −800 to 1100 mV/SCE at scan rates of 1 mV/s. Corrosion current density (I_{corr}) and corrosion potential (E_{corr}) were derived from the linear Tafel segment of anodic and cathodic curves.

All electrochemical experiments were carried out in a three-electrode electrochemical cell consisting of graphite as counter electrode, silver/silver chloride as reference and the coated steel sample as working electrode. Experiments were made at least in duplicated samples.

3. Results and discussion

3.1. Physico-chemical characterization

3.1.1. Morphology and structural analysis

The XRD pattern of pristine CONPs as shown in Fig. 2(a) revealed the crystalline nature of the particles and the characteristic peaks observed at 28.53°, 33.09°, 47.5°, 56.26° could be assigned, respectively, to the 111, 200, 220, 311 crystal planes [17] in accordance with JCPDS No: 34-0394 of CeO_2 crystal. The XRD pattern for CONPs loaded with GA remained similar to the CONPs without GA and the absence of any additional peak(s) revealing that the presence of GA did not induce relevant structural changes in the CONPs.

Fourier transform infrared microscopy (FTIR) analysis was carried out to confirm the chemical composition of CONPs before and after loading with GA (Fig. 2(b)). The characteristic stretching vibrations of CeO_2 (O—Ce—O) could be observed at 557 cm^{-1} [17]. The broadband at 3400–3300 cm^{-1} evidenced the stretching vibration of O—H, and the band at 2917 cm^{-1} could be assigned to the stretching vibration of C—H due to the presence of sugars, arabinose, and galactose [29]. The absorption band of very low intensity at 2310 cm^{-1} has been usually assigned to CO_2 vibration. The bands at 1608 cm^{-1} and 1413 cm^{-1} could be assigned to the asymmetric and symmetric stretching of COO^- [30]. The 1413 cm^{-1} band corresponds to C—N stretching vibration, which confirms the loading of GA into CONPs. The bands in the range of 1200–900 cm^{-1} represented the fingerprints of carbohydrates. A distinct band at 1030 cm^{-1}, was assigned to the alkene C—H bend from polysaccharides [22]. The band at 900–500 cm^{-1} was due to CCO and COC. Comparison of the characteristic peaks observed in the CONPs, GA, and CONPs loaded with GA confirmed the loading of GA into CONPs. Table 1 shows the characteristic band for CONPs loaded with GA at different wavenumbers.

The morphology of CONPs and CONPs loaded with GA was investigated with a high resolution transmission electron microscope (HR-TEM). The images depicted in Fig. 3(a, b) indicate that the average size of pristine CONPs is typically below 20 nm and that they possess cubic

Table 1
Characteristic bands.

Sr. No	Band at wavenumber (cm^{-1})	Nature	Ref.
1	3400–3300	Stretching vibration of O—H	[31]
2	2917	Stretching vibration of C—H	[32]
3	1413	Stretching vibration C—N	[33]
4	1200–900	Fingerprints of Carbohydrates	[34]

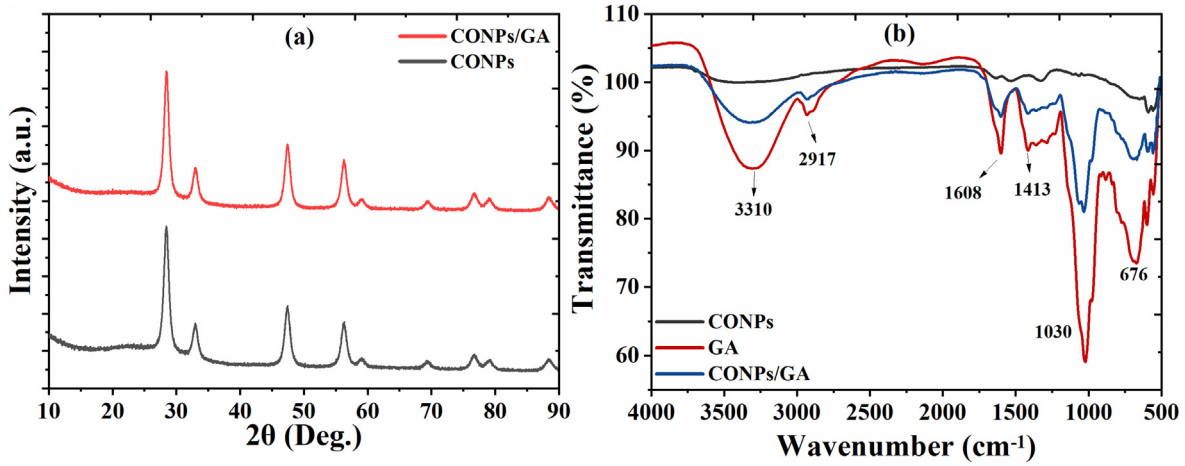

Fig. 2. (a) XRD patterns of pristine CONPs and CONPs loaded with GA and (b) FTIR analysis of CONPs, GA, and CONPs loaded with GA.

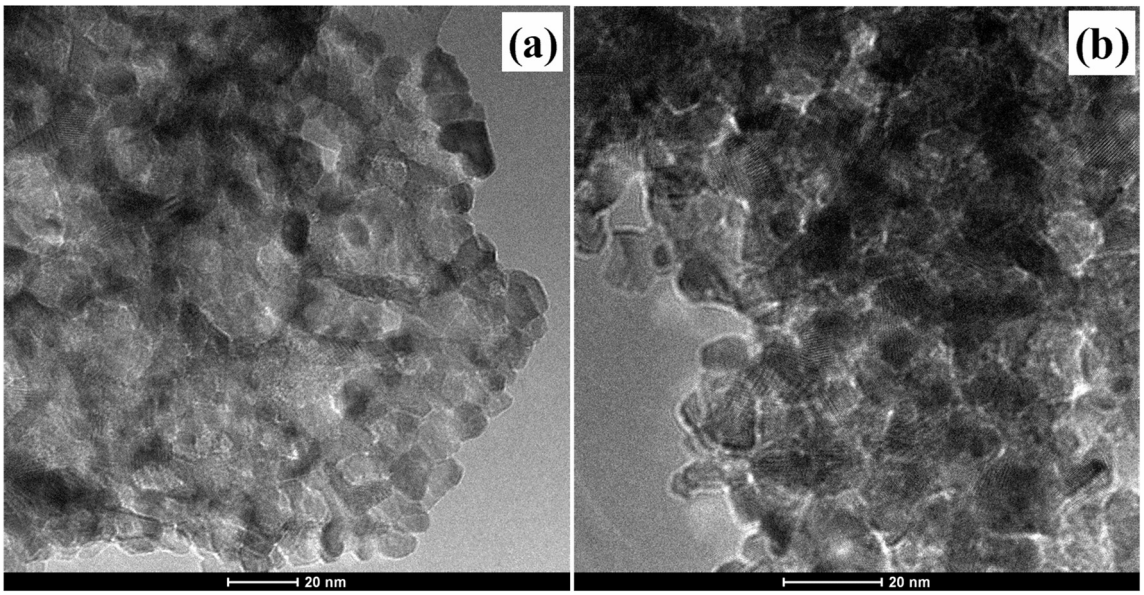

Fig. 3. HR-TEM images: (a) pristine CONPs (b) CONPs loaded with GA.

structure and some porosity. The darker areas in Fig. 3(b) can be attributed to the loading of CONPs with GA. Furthermore, no relevant agglomerations could be noticed.

3.1.2. Thermal gravitational analysis (TGA)

Thermal gravimetric analysis (TGA and DTA) of CONPs and CONPs loaded with GA is shown in Fig. 4(a, b). The thermal analysis allowed to assess the thermal stability and loading capacity of CONPs with GA. The pristine CONPs show no significant weight loss and remained stable at all stages, confirming excellent thermal stability owing to its high melting point is ~3500 °C. However, in the case of CONPs loaded with GA, the initial weight loss observed till 120 °C was due to the removal of moisture in the 1st stage (room temperature to 200 °C) [35]. During the 2nd stage (200–400 °C), as the temperature increased from 200 °C, a significant weight loss occurred due to decomposition of GA, probably the polysaccharides [30], since GA contains carboxylate and carboxylic acid functional groups [36]. Finally, in the 3rd stage (400–600 °C), a gradual weight loss was observed. The DTA curve for CONPs/GA is nearly constant and no sharp peaks were observed because CONPs has a high melting point and it shows no weight loss and remain stable till 600 °C. The two peaks observed for CONPs/GA include a 1st one assigned to removal of moisture content from CONPs/GA and a 2nd one around 300 °C due to decomposition of GA. Overall, the 40 wt % loss observed seemed to include the 10.0 wt% due to the moisture and 30 wt% due to decomposition of GA. Thus, the TGA results suggest that ~30.0 wt% GA has been loaded into CONPs, which is a reasonable loading capacity.

3.1.3. BET analysis

The BET results are depicted in Fig. 5. The specific surface area (SSA) and calculated cumulative pore volume of the pristine CONPs were determined and were 137.966 m^2g^{-1} and 0.515237 ccg^{-1}, respectively. However, when GA was loaded on the CONPs, the SSA was reduced to 31.070 m^2g^{-1}, and the pore volume also decreased to 0.132497 ccg^{-1}, which demonstrated the efficient loading of GA into CONPs in agreement with the previous TGA results (Fig. 4(a,b)).

3.2. Anti-corrosion properties

3.2.1. Electrochemical impedance spectroscopy (EIS)

The corrosion resistance of the reference coatings (containing CONPs without inhibitor) and modified coatings (containing CONPs

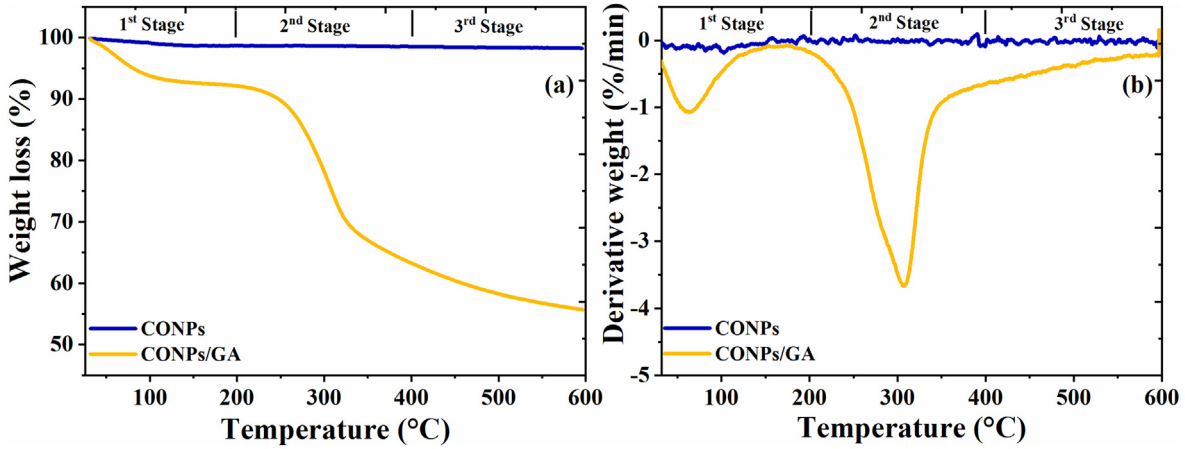

Fig. 4. (a) TGA and (b) DTA curves of pristine CONPs and CONPs loaded with GA.

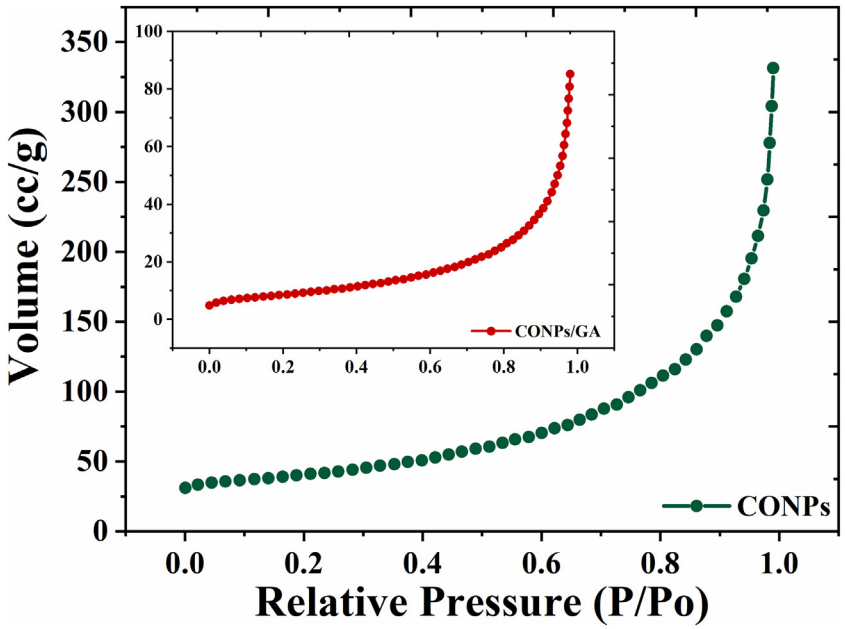

Fig. 5. BET analysis of pristine CONPs and CONPs loaded with GA.

loaded with GA), applied on steel substrates, was investigated by EIS for 15 days immersion in 3.5 wt% NaCl at room temperature. A controlled scratch was made in the coatings to assess the corrosion protection ability of CONPs loaded with GA. The scratched area of coatings and photographs of reference and modified coating after corrosion test provided in (Fig. S1). The impedance spectra for steel samples protected with the reference coatings are depicted in Fig. 6(a, b). The coated samples showed a capacitive response in the high frequency region,

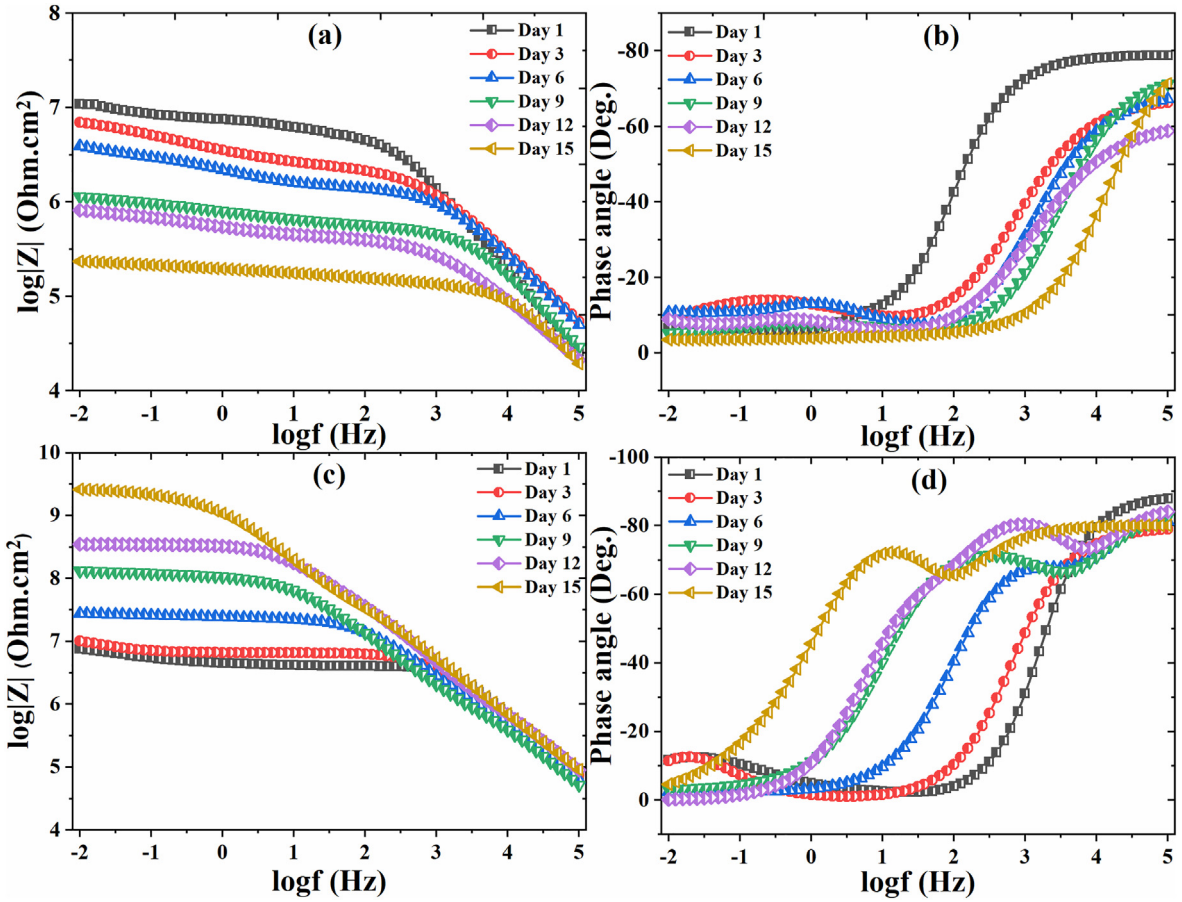

Fig. 6. EIS Bode plots for (a, b) Reference and (c, d) Modified coating.

assigned to the impedance of the intact part of the coating, which decreased over time due to electrolyte uptake and delamination of the coating from the defect. This is also clearly illustrated by the phase angle evolution and poorest definition of the high-frequency time constant over time. At lower frequencies the presence of a time constant accounts for the corrosion activity at the steel surface. The total impedance values of the reference coatings reached ~20 MΩ cm^2 on the 1st day of immersion and slowly decreased with time due to the progress of corrosion activity at the exposed steel (the coating was previously scratched). The overall impedance values decreased approximately two orders of magnitude after 15 days immersion, due to the progress of corrosion.

Comparatively, the coatings modified with the CONPs loaded with GA revealed an opposite trend. Initially, the overall impedance values were close to 10 MΩ cm^2 and a well-defined time constant, assigned to corrosion activity was visible at low frequencies, while the high-frequency time constant was visible at frequencies above 10 kHz. However, over time, the impedance increased for more than 2 orders of magnitude and this increase was accompanied by the disappearance of the low-frequency time constant and by the broadening of the high-frequency one - Fig. 6(c, d). The impedance values reached 2.16 GΩ cm^2 on 15th day of immersion and the low-frequency time constant vanished, suggesting that corrosion activity at the exposed steel surface was mitigated. A possible explanation is that presence of GA aids on the formation a protective layer on the steel substrate [37]. Moreover, in a first analysis, it seems to promote the recovery of the protective properties of the coating since there is a significant broadening of the phase angle in the high frequency region.

The EIS parameter values after fitting EIS data with equivalent circuit are depicted in Fig. 7. The pore resistance (R_{po}) on 1st day of immersion is measured ~2 M Ω cm^2 for the reference coating, and it remains stable for a couple of days, then it decreases slightly with the increase in immersion time as shown in the Fig. 7(b). However, the pore resistance (R_{po}) of modified coatings increasing with immersion time because CONPs-GA as filler material helps to reduce the number of pores and conductive paths in the epoxy. The better inhibition provided by GA that helps to improve barrier properties of coating that makes it stable against corrosion. The value of R_{po} for modified coatings is increased to 415 MΩ cm^2 after 15th day of immersion as compared to the reference coating, which is reduced to 39.4 KΩ cm^2.

The charge transfer resistance (R_{ct}) of reference and modified coatings are depicted in Fig. 7(c). The value of R_{ct} for reference and modified coatings is ~10^7 Ω cm^2 on 1st day of immersion, but the value for R_{ct} of the reference coatings gradually decreases with increasing time due to lack of inhibition and reduced by one order magnitude after one week of immersion. Contrary to this, the value of R_{ct} increases with time for the modified coatings due to better inhibition of GA. The self-release of loaded GA from CONPs leads to its adsorption on the steel substrate and form a protective layer, which helps to isolate the steel substrate

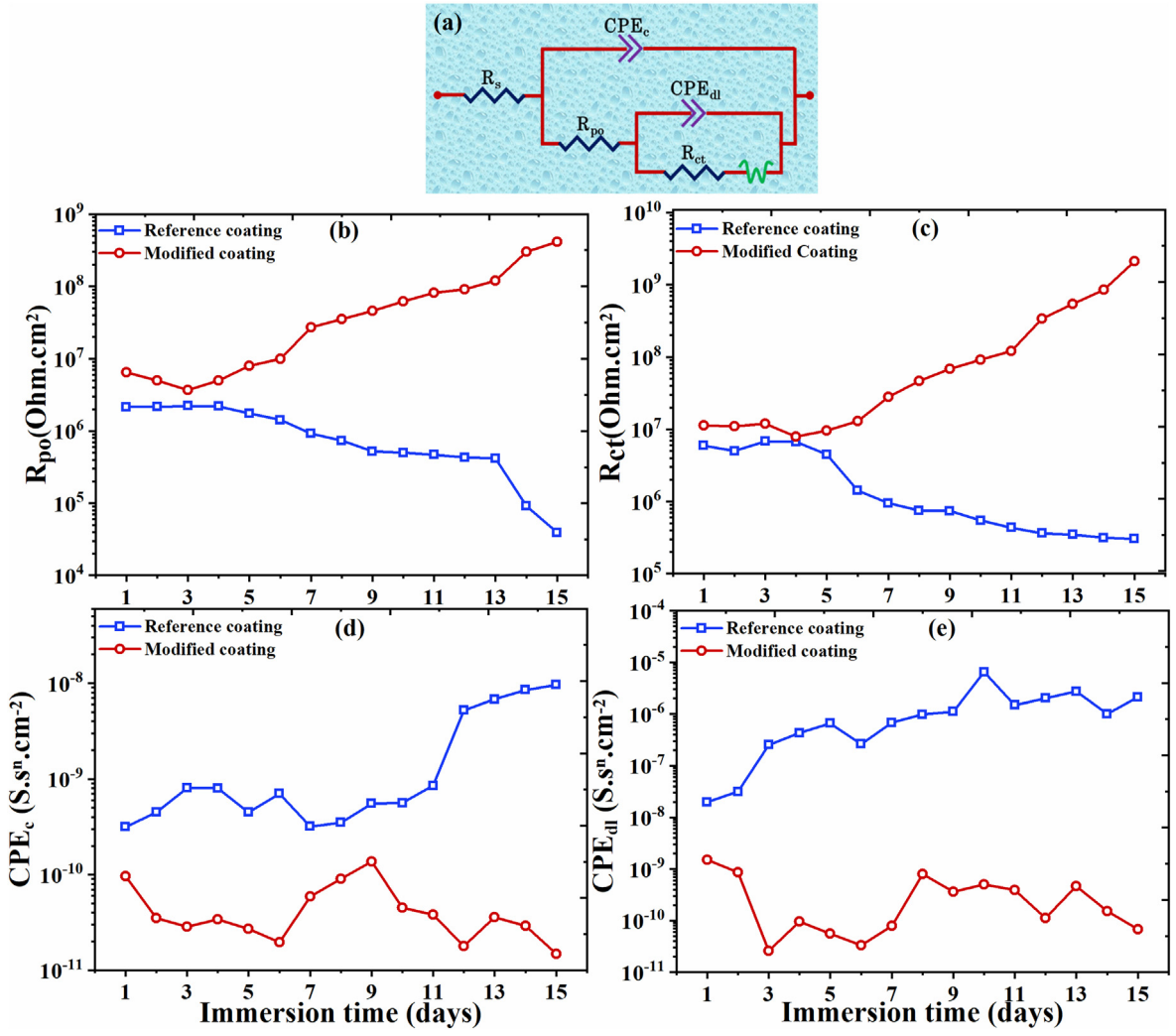

Fig. 7. (a) Equivalent circuit and EIS parameters values after fitting with equivalent circuit (b) Pore resistance (R_{po}) (c) Charge transfer resistance (R_{ct}) (d) Coating capacitance (CPE_c) and (e) Double layer capacitance (CPE_{dl}).

from the electrolyte [38]. The charge transfer resistance (R_{ct}) value of modified coatings is reached to 2.165×10^9 Ω cm^2 on 15th days of immersion compared to 305.7×10^3 Ω cm^2 for the reference coatings. These findings demonstrate better corrosion inhibition efficiency of modified coatings. The improvement in charge transfer resistance (R_{ct}) is also consistent with the increase in pore resistance (R_{po}) of the modified coatings.

The constant phase element (CPE_c) value for reference and the modified coatings is given in Fig. 7(d). The CPE_c value for reference coatings increases with time due to more conductive paths in reference coatings, and thus the capacitance value increases gradually. As the electrolyte comes in contact with epoxy coatings, more conducting paths are there due to the absence of inhibition against corrosion. While in the case of modified coatings, the value for CPE_c remains stable as compared to the reference coatings due to better inhibition efficiency provided by the GA. The lower value of CPE_c with a higher value of corrosion resistance indicates the superior corrosion resistance of the modified coating [39]. The low admittance value of CPE_{dl} for modified coatings as compared to the reference coatings Fig. 7(e)further provides strong evidence to the improved anti-corrosion properties of modified coatings.

For comparative purpose, the impedance values for reference and modified coating evaluated from EIS measurements are also provided in Table 2. The inhibition efficiency (I.E%) of the modified coating was evaluation from Eq. (1) [40], and calculated value of (I.E%) provided in the Table 2.

$$\text{I.E}\ (\%) = (1 - R_{ct}/R_{ct1}) \times 100 \quad (1)$$

where R_{ct} is the charge transfer resistance in the absence of inhibitor (GA), while R_{ct1} is the charge transfer resistance of the modified coatings. The impedance value for reference coatings dropped by two orders of magnitude from 12 MΩ cm^2 to 300 KΩ cm^2 after 15 days of immersion, while the values for the CONPS+GA - modified coating increased by two orders magnitude from 6 MΩ cm^2 to values close to 2.16 GΩ cm^2 after 15 days of immersion. The increase in the impedance values evidenced an important recovery of the low-frequency impedance that can be assigned to the formation of a protective layer over the exposed steel.

The steel substrate coated with the modified coating (CONPs-GA) showed good corrosion resistance probably due to the good dispersion of ceria in the epoxy matrix and its possible interaction with active sites of cured epoxy [41,42] probably via Lewis Acid-base interactions between CeO_2 and the epoxy. Previously, it was reported that Gum Arabic microcapsules can work as filler in coatings, blocking micro-pores in the epoxy matrix and providing polymer healing and improved corrosion resistance [43]. It is therefore expectable that the use of Gum Arabic loaded into ceria enhances the epoxy barrier properties due to better crosslinking of the cured epoxy. That helps to improve the anti-corrosive properties. Ultimately, the presence of CeO_2 nanoparticles with Gum Arabic reduces the pores available for water uptake and eliminates conductive paths in the epoxy coating increasing its barrier properties. To better evaluate this effect the impedance response of non-damaged coatings was also studied and a set of representative spectra shown in Fig. 8(a, b). The evolution of the low-frequency impedance over time is depicted in Fig. 8c.

Table 2
Impedance values and protection efficiency for the reference and CONPS+GA - modified coatings at various immersion time.

Immersion time (days)	Impedance value Z_{max} (MΩ cm^2)		
	Reference coating	Modified coating	I.E(%)
1	11.9 ± 0.7	5.95 ± 0.6	–
3	6.68 ± 0.7	11.4 ± 0.4	50.4
6	1.42 ± 1.2	13.4 ± 1.4	54.2
9	0.74 ± 0.3	69.8 ± 1.1	91.3
12	0.36 ± 0.2	344 ± 0.3	98.2
15	0.31 ± 0.1	2160 ± 0.2	99.7

The non-damaged coated samples evidenced a well-defined capacitive response at high frequencies, with very stable phase angle values that evidenced very good barrier properties. Interestingly, over time there were a two orders of magnitude increase of the overall impedance values. Typically, it would be expected an impedance decrease as a consequence of water uptake and the initiation of corrosion activity at the steel coating interface. However, in this case – Fig. 7, the opposite trend is clearly observed. This reflects that the coating barrier properties improved during immersion and this is a consequence of the presence of GA that is able to block pores formed in the coating and to preserve the steel interface from corrosion. This effect, on the one hand delays coating delamination at bottom of pores and, on the other hand seems to repair pores and defects in the coating. This supports the impedance evolution observed in the spectra for the coatings containing a defect. As result, there is an important recovery over time as illustrated in Fig. 8.

3.2.2. Potentiodynamic polarization curves

The impedance results clearly indicate that GA has a very beneficial impact on the coating protective properties, aiding to the recovery of the barrier properties. However, given the high impedance values, the role at the level of steel surface was hard to discriminate. For that purpose, an additional set of experiments, using uncoated steel exposed to a NaCl solution containing GA, was performed. The electrochemical response of steel (uncoated samples) immersed in 3.5 wt% NaCl solution in the absence and presence of Gum Arabic after different immersion times was studied by d.c. polarization and the results are depicted in Fig. 9. Relevant parameters such as corrosion potential (E_{corr}), current density (I_{corr}), and corrosion rates were calculated from the Tafel slopes - Table 3.

The E_{corr} value determined on the steel substrate after immersion in the NaCl in the absence of GA was ~ −862 mV and increased to more anodic values (~−642 mV in the presence of GA) – Table 3 [38]. The shift in E_{corr} value with respect to the blank steel is more than 85 mV which suggests an anodic inhibition effect of GA [44]. For longer immersion times, the corrosion potential (E_{corr}) continuously shifted towards more noble values, reaching approximately −500 mV in the presence of GA. This shift indicates that the inhibitor molecules could be adsorbed onto the steel substrate, inhibiting the anodic reaction. The anodic and cathodic curves shift towards lower current densities in the presence of GA, which suggests a decrease in the corrosion active areas [45]. The current density (I_{corr}) decreased more than one order of magnitude with the immersion time in the presence of GA. The inhibition efficiency (IE) for potentiodynamic polarization curves can be calculated by the following equation [46].

$$\text{Inhibition efficiency}\ (\text{IE}\%) = (1 - i_{corr2}/i_{corr1}) \times 100$$

in which I_{corr2} is the current density of steel in presence of GA and I_{corr1} is the current density of steel in absence of GA. Thus, a decrease in the current density value is due to a better inhibition effect of GA and to a diminution of the active area. The maximum 76% of corrosion inhibition efficiency was calculated after 24 h of immersion in GA.

The results confirmed the corrosion inhibition role of GA over the steel surface. The evolution of the anodic and cathodic Tafel slopes suggest a mixed corrosion inhibition mechanism, but the evolution of the corrosion potential evolution points out the predominance of thr anodic corrosion inhibition effect.

3.3. Post potentiodynamic polarization analyses

3.3.1. SEM/EDS analysis

In order to study the detail morphology and composition of the steel surface and to confirm the adsorption of GA on the steel substrate, SEM and EDS elemental mapping images of the steel substrates immersed

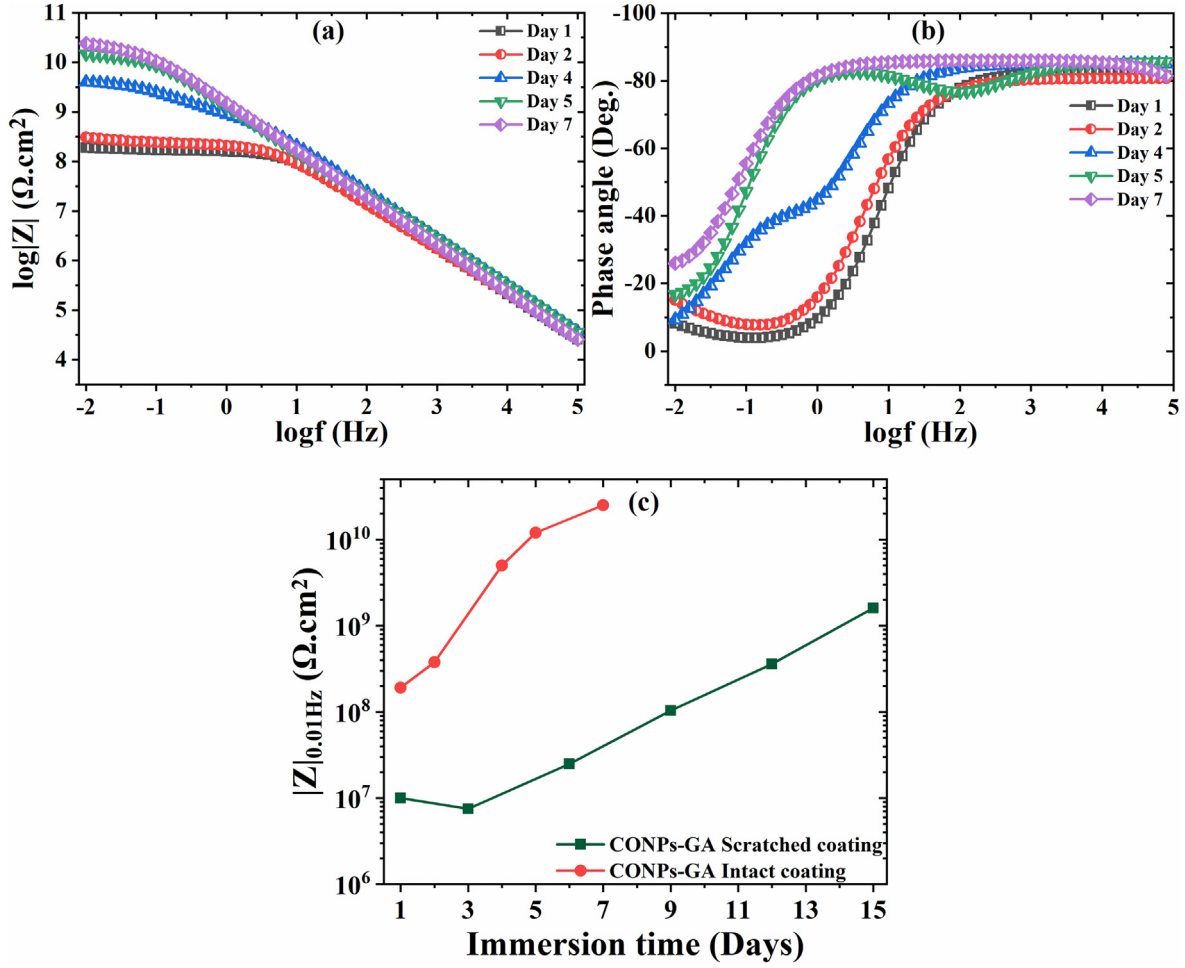

Fig. 8. (a, b) EIS Bode plots for the coating modified with CONPs and GA over 7 days of immersion, (c) Evolution of the low-frequency impedance over time of CONPs and GA intact coating.

into 3.5% NaCl solution, in the presence and absence of GA are shown in Fig. 10.

The steel surface in the absence of GA (Fig. 10(a)) reveals the formation of nearly spherical precipitates composed of iron and oxygen covering the entire surface and that reveal the formation of a uniform layer of corrosion products. In the presence of GA these features were almost absent and a relatively uniform layer seems deposited onto the surface, (Fig. 10(b)). The elemental mapping (Fig. 10(b)) shows traces of nitrogen (N) and sodium (Na) on the surface of the steel substrates immersed into the solution containing GA, which confirms the presence of GA at the surface. The presence of nitrogen (N) in presence of GA (Fig. 10 (b indicated the formation of a GA-containing protective layer.

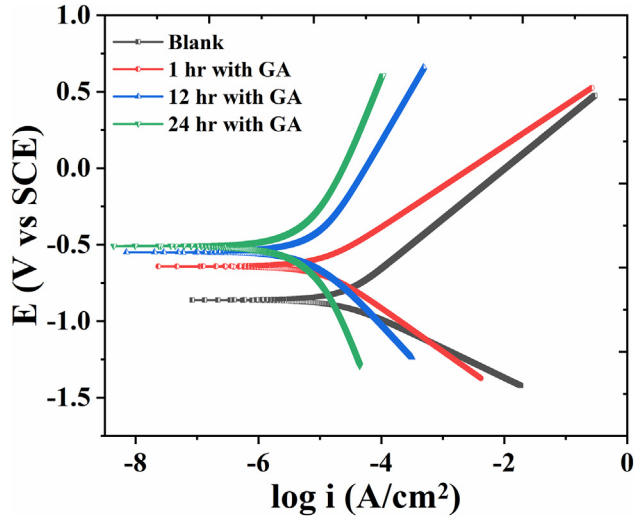

Fig. 9. Potentiodynamic polarization curves obtained for blank steel substrate exposed to NaCl solutions, with and without the presence of GA at different immersion times.

3.3.2. Atomic force microscopy (AFM) analysis

The Atomic force microscopy (AFM) analysis was used to measure the roughness of the blank steel immersed into the 3.5 wt% NaCl solution in the absence and presence of GA after the polarization tests. 3-D AFM images and their corresponding surface roughness profiles of steel substrates are presented in Fig. 11(a). A comparison of the 3D AFM images (Fig. 11(b)) indicated that the steel surface is relatively smooth in the presence of GA when compared to the surface in the absence of GA. The surface roughness (R.M.S) value of the steel in the

Table 3
Potentiodynamic polarization parameters obtained from Tafel plots.

Sample	E_{corr} (mV)	I_{corr} (μAcm^{-2})	Efficiency (%)	Corrosion rate
Blank	−862	24.10	–	11.0 mpy
1 h with GA	−642	11.10	54	5.068 mpy
12 h with GA	−550	8.620	64	4.102 mpy
24 h with GA	−508	5.690	76	3.487 mpy

absence of GA is (RMS = 62.702), which is reduced to (R.M.S. = 31.069) in the presence of GA (Fig. 11). These findings are consistent with the FE-SEM analysis presented in Fig. 10(a,b). The reduction in the surface roughness value in the presence of GA can be attributed to the formation of a protective layer at the surface of the steel substrate. These findings are also consistent with previous studies [47].

3.4. Corrosion protection mechanism

As discussed in the previous section, the enhanced corrosion protection effect can be primarily attributed to the presence of GA onto the CONPs. Gum Arabic has a negative charge on its surface as measured by Zeta potential (Fig. S2), which facilitates the adsorption of these negatively charged species (GA) over the positively charged metal surface [24].

The first important aspect is that GA acts as corrosion inhibitor, displaying predominantly an anodic inhibition mechanism. Literature reports that GA is a polysaccharide containing functionalities that are able to establish either physical or chemical adsorption at the steel surface. The corrosion inhibition efficiency of GA can be attributed to its amphiphilic nature (ability to demonstrate both hydrophilic and hydrophobic character). The hydrophilic nature of GA is due to the polysaccharides functional groups, which are highly water-soluble due to the presence of hydroxyl (-OH) and carboxyl (-COOH) functional groups. In contrast, the hydrophobic behavior of GA is due to the presence of protein-rich fractions. On the one hand, the hydroxyl groups can be protonated in acidic media (formed at anodic sites as a consequence of Fe cations hydrolysis) trapping chloride anions [48], that are attracted to surface, inhibiting its accumulation on the steel surface. On the other hand, GA molecules can adsorb onto the steel surface via the lone

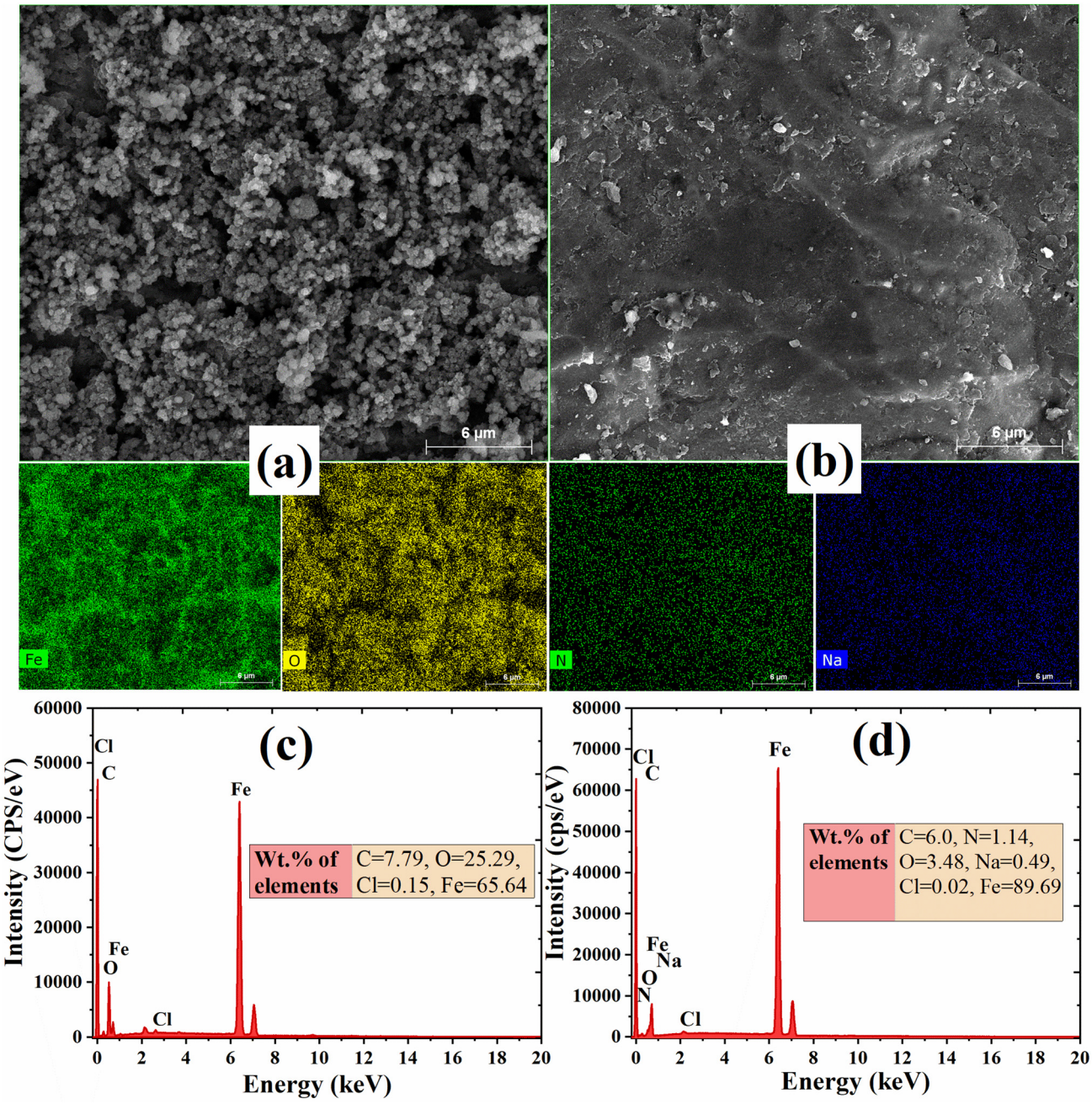

Fig. 10. Post potentiodynamic FE-SEM, elemental mapping, and EDS analysis of blank steel exposed to NaCl solutions in the (a,c) absence and (b, d) presence of GA.

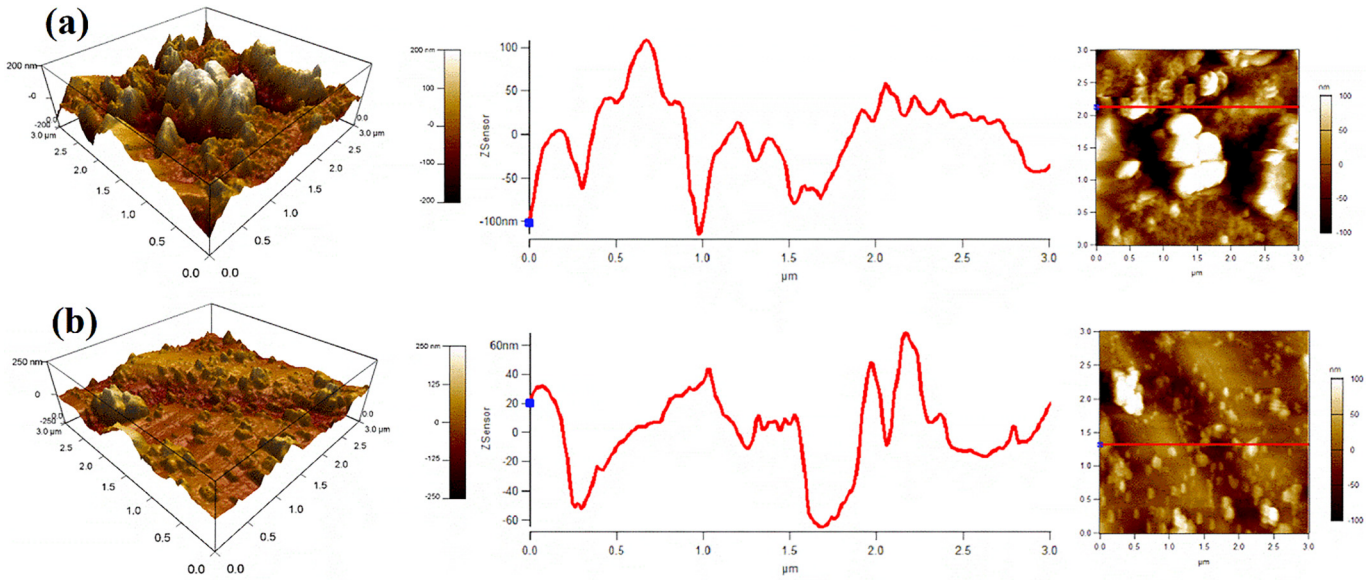

Fig. 11. Post potentiodynamic AFM analysis of the steel substrates immersed into 3.5% NaCl solution in the (a) absence and (b) presence of GA.

pairs of electrons in the heteroatoms forming a stable surface layer [49]. The formation of carbohydrate-iron complexes is also a possibility that has been discussed and that cannot be fully discarded [50]. If so, these complexes may form a stable surface layer that further prevents iron dissolution. In fact, the changes in the anodic Tafel slopes seem more pronounced compared to the cathodic ones, which suggests that the formation of GA and iron complexes might occur. Previous results also suggest that chemisorption is responsible for the anodic inhibition effect observed [51]. Therefore, it can be concluded that the improved corrosion resistance involves different mechanisms that, overall contribute to the enhanced corrosion protection effect.

The proposed inhibition mechanism in coated samples can be schematically represented in Fig. 12. GA covering the CONPs can adsorb on the steel surface via a chemisorption mechanism that involves donor-acceptor interactions between the lone electron pairs as well as pi-electrons from the aromatic rings and the vacant d-orbitals of Fe. This leads to the formation of a stable surface film, where both GA and CeO_2 contribute to an effective corrosion inhibition effect. Moreover, protonated species, at the anodic sites, may trap chlorides preventing them to complex with iron cations. To summarize, the inhibition mechanism in coated samples is likely to involve both physical and chemical adoption of corrosion inhibitor at the steel surface.

In addition to the anodic corrosion inhibition effect, GA also improves the epoxy coating barrier properties. While CeO_2 enhances the barrier properties due to the better crosslinking of cured epoxy, GA helps to decrease micro porosities in the epoxy matrix. This is supported by the fact that Gum Arabic has already been used as filler material in epoxy [43] and thus, the use of Gum Arabic loaded into ceria reduces the number of pores and conductive paths in epoxy, which leads to the increase and recovery overtime of the epoxy coating barrier properties.

4. Conclusion

Eco-friendly Gum Arabic (GA) was used as a corrosion inhibitor and loaded into cerium oxide nanoparticles (CONPs) to protect epoxy coated steel parts. Electrochemical impedance spectroscopy (EIS) reveal the excellent anti-corrosion properties of the coatings modified with ceria nanoparticles and GA when compared to the reference coatings without GA addition. An important recovery of the coating barrier properties could be observed in the presence of GA. The improvement in barrier properties of modified coating is due to better crosslinking of cured epoxy that leads to the decrease in the number of pores and conducting paths. The Gum Arabic released from CONPs, and adsorbed on steel substrate helps to reduce the active area of corrosion and provide corrosion inhibition. The inhibition mechanism is likely to involve both physical and chemical adoption of GA at the steel surface and a marked anodic inhibition effect as demonstrated by the potentiodynamic polarization tests.

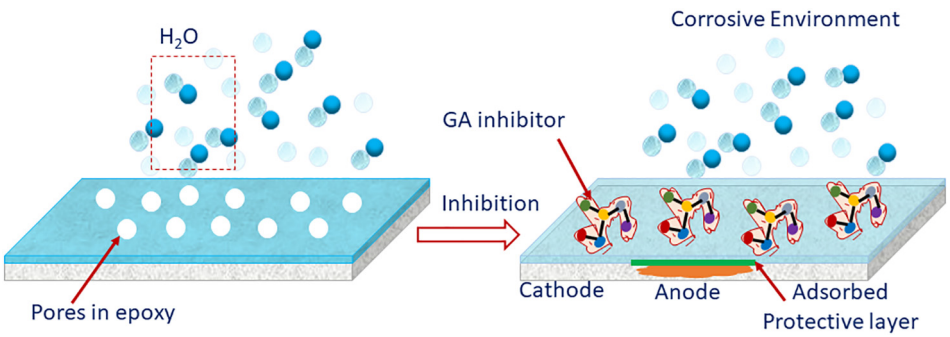

Fig. 12. Schematic diagram showing the corrosion inhibition mechanism of GA in the modified coatings.

Credit Author Statement

Muddasir Nawaz: Conceptualization, Methodology, Validation, Formal analysis, Investigation, Writing – Original Draft **R. A Shakoor:** Supervision, Writing – Review & Editing, Project administration, Resources **Ramazan Kahraman:** Resources, Funding acquisition **M. F. Montemor:** Validation, Writing – Review & Editing, Funding acquisition

Declaration of Competing Interest

The authors declare that they have no known competing financial interests or personal relationships that could have appeared to influence the work reported in this paper.

Acknowledgement

This publication was made possible by NPRP11S-1226-170132 from Qatar National Research Fund (a member of the Qatar Foundation). Statements made herein are solely the responsibility of the authors. The authors would like to thanks to the Central Laboratories Unit (CLU), Qatar University, 2713, Doha, Qatar for FE-SEM, and HR-TEM analyses. Authors from Portugal acknowledge FCT for the additional funding under the project UIDB/00100/2020 and UIDP/00100/2020. Open Access funding provided by the Qatar National Library.

Data availability statement

The raw data required to reproduce these findings cannot be shared at this time as the data also forms part of an ongoing study.

Appendix A. Supplementary data

Supplementary data to this article can be found online at https://doi.org/10.1016/j.matdes.2020.109361.

References

[1] J.D. Bray, A. Rodriguez-Marek, J.L. Gillie, Design ground motions near active faults, Bull. New Zeal. Soc. Earthq. Eng. 42 (2009) 1–8, https://doi.org/10.5459/bnzsee.42.1.1-8.

[2] M.L. Zheludkevich, D.G. Shchukin, K.A. Yasakau, H. Möhwald, M.G.S. Ferreira, Anticorrosion coatings with self-healing effect based on nanocontainers impregnated with corrosion inhibitor, Chem. Mater. 19 (2007) 402–411, https://doi.org/10.1021/cm062066k.

[3] M.F. Montemor, Functional and smart coatings for corrosion protection: a review of recent advances, Surf. Coatings Technol. 258 (2014) 17–37, https://doi.org/10.1016/j.surfcoat.2014.06.031.

[4] M. Nawaz, N. Yusuf, S. Habib, R.A. Shakoor, F. Ubaid, Z. Ahmad, R. Kahraman, S. Mansour, W. Gao, Development and properties of polymeric nanocomposite coatings, Polymers (Basel) 11 (2019)https://doi.org/10.3390/polym11050852.

[5] M.L. Zheludkevich, J. Tedim, M.G.S. Ferreira, "Smart" coatings for active corrosion protection based on multi-functional micro and nanocontainers, Electrochim. Acta 82 (2012) 314–323, https://doi.org/10.1016/j.electacta.2012.04.095.

[6] M. Nawaz, S. Habib, A. Khan, R.A. Shakoor, R. Kahraman, Autonomous self-healing in epoxy coatings, (2020). doi:https://doi.org/10.1039/c9nj06436b.

[7] A. Pepe, M. Aparicio, S. Ceré, A. Durán, Preparation and characterization of cerium doped silica sol-gel coatings on glass and aluminum substrates, J. Non-Cryst. Solids 348 (2004) 162–171, https://doi.org/10.1016/j.jnoncrysol.2004.08.141.

[8] M. Attaei, L.M. Calado, M.G. Taryba, Y. Morozov, R.A. Shakoor, R. Kahraman, A.C. Marques, M.F. Montemor, Autonomous self-healing in epoxy coatings provided by high efficiency isophorone diisocyanate (IPDI) microcapsules for protection of carbon steel, Prog. Org. Coat. 139 (2020) 105445, https://doi.org/10.1016/j.porgcoat.2019.105445.

[9] D.G. Bekas, K. Tsirka, D. Baltzis, A.S. Paipetis, Self-healing materials: a review of advances in materials, evaluation, characterization and monitoring techniques, Compos. Part B Eng. 87 (2016) 92–119, https://doi.org/10.1016/j.compositesb.2015.09.057.

[10] F. Zhang, P. Ju, M. Pan, D. Zhang, Y. Huang, G. Li, X. Li, Self-healing mechanisms in smart protective coatings: a review, Corros. Sci. 144 (2018) 74–88, https://doi.org/10.1016/j.corsci.2018.08.005.

[11] R. Raj, Y. Morozov, L.M. Calado, M.G. Taryba, R. Kahraman, A. Shakoor, M.F. Montemor, Inhibitor loaded calcium carbonate microparticles for corrosion protection of epoxy-coated carbon steel, Electrochim. Acta 319 (2019) 801–812, https://doi.org/10.1016/j.electacta.2019.07.059.

[12] A. Khan, A. Hassanein, S. Habib, M. Nawaz, R.A. Shakoor, R. Kahraman, Hybrid Halloysite nanotubes as smart carriers for corrosion protection, ACS Appl. Mater. Interfaces 12 (2020) 37571–37584, https://doi.org/10.1021/acsami.0c08953.

[13] P. Poornima Vijayan, M. Al-Maadeed, Self-repairing composites for corrosion protection: A review on recent strategies and evaluation methods, Materials (Basel) 12 (2019)https://doi.org/10.3390/ma12172754.

[14] A.E. Hughes, I.S. Cole, T.H. Muster, R.J. Varley, Designing green, self-healing coatings for metal protection, NPG Asia Mater. 2 (2010) 143–151, https://doi.org/10.1038/asiamat.2010.136.

[15] M.H. Sliem, M. Afifi, A. Bahgat Radwan, E.M. Fayyad, M.F. Shibl, F.E.T. Heakal, A.M. Abdullah, AEO7 surfactant as an eco-friendly corrosion inhibitor for carbon steel in HCl solution, Sci. Rep. 9 (2019) 1–16, https://doi.org/10.1038/s41598-018-37254-7.

[16] M. Mauro, M. Crosera, M. Monai, T. Montini, P. Fornasiero, M. Bovenzi, G. Adami, G. Turco, F.L. Filon, Cerium oxide nanoparticles absorption through intact and damaged human skin, Molecules 24 (2019) 1–10, https://doi.org/10.3390/molecules24203759.

[17] D.M.D.M. Prabaharan, K. Sadaiyandi, M. Mahendran, S. Sagadevan, Structural, optical, morphological and dielectric properties of cerium oxide nanoparticles, Mater. Res. 19 (2016) 478–482, https://doi.org/10.1590/1980-5373-MR-2015-0698.

[18] M. Taryba, S.V. Lamaka, D. Snihirova, M.G.S. Ferreira, M.F. Montemor, W.K. Wijting, S. Toews, G. Grundmeier, The combined use of scanning vibrating electrode technique and micro-potentiometry to assess the self-repair processes in defects on "smart" coatings applied to galvanized steel, Electrochim. Acta 56 (2011) 4475–4488, https://doi.org/10.1016/j.electacta.2011.02.048.

[19] M.F. Montemor, R. Pinto, M.G.S. Ferreira, Chemical composition and corrosion protection of silane films modified with CeO2 nanoparticles, Electrochim. Acta 54 (2009) 5179–5189, https://doi.org/10.1016/j.electacta.2009.01.053.

[20] L.G. Ecco, Waterborne Paint System Based on CeO_2 and Polyaniline Nanoparticles for Anticorrosion Protection of Steel, 2014 1–116.

[21] S. Habib, E. Fayyad, M. Nawaz, A. Khan, R.A. Shakoor, R. Kahraman, A. Abdullah, Cerium dioxide nanoparticles as smart carriers for self-healing coatings, Nanomaterials. 10 (2020) 1–4, https://doi.org/10.3390/nano10040791.

[22] M.A. Abu-Dalo, A.A. Othman, N.A.F. Al-Rawashdeh, Exudate gum from acacia trees as green corrosion inhibitor for mild steel in acidic media, Int. J. Electrochem. Sci. 7 (2012) 9303–9324.

[23] M.L. Zheludkevich, J. Tedim, C.S.R. Freire, S.C.M. Fernandes, S. Kallip, A. Lisenkov, A. Gandini, M.G.S. Ferreira, Self-healing protective coatings with "green" chitosan based pre-layer reservoir of corrosion inhibitor, J. Mater. Chem. 21 (2011) 4805–4812, https://doi.org/10.1039/c1jm10304k.

[24] C. Shen, V. Alvarez, J.D.B. Koenig, J.L. Luo, Gum Arabic as corrosion inhibitor in the oil industry: experimental and theoretical studies, Corros. Eng. Sci. Technol. 54 (2019) 444–454, https://doi.org/10.1080/1478422X.2019.1613780.

[25] A. Peter, I.B. Obot, S.K. Sharma, Use of natural gums as green corrosion inhibitors: an overview, Int. J. Ind. Chem. 6 (2015) 153–164, https://doi.org/10.1007/s40090-015-0040-1.

[26] G. Palumbo, K. Berent, E. Proniewicz, J. Banaś, Guar gum as an eco-friendly corrosion inhibitor for pure aluminium in 1-M HCl solution, Materials (Basel) 12 (2019) https://doi.org/10.3390/ma12162620.

[27] K. Azzaoui, E. Mejdoubi, S. Jodeh, A. Lamhamdi, E. Rodriguez-Castellón, M. Algarra, A. Zarrouk, A. Errich, R. Salghi, H. Lgaz, Eco friendly green inhibitor Gum Arabic (GA) for the corrosion control of mild steel in hydrochloric acid medium, Corros. Sci. 129 (2017) 70–81, https://doi.org/10.1016/j.corsci.2017.09.027.

[28] H. Bentrah, Y. Rahali, A. Chala, Gum Arabic as an eco-friendly inhibitor for API 5L X42 pipeline steel in HCl medium, Corros. Sci. 82 (2014) 426–431, https://doi.org/10.1016/j.corsci.2013.12.018.

[29] M.M. Solomon, H. Gerengi, S.A. Umoren, N.B. Essien, U.B. Essien, E. Kaya, Gum Arabic-silver nanoparticles composite as a green anticorrosive formulation for steel corrosion in strong acid media, Carbohydr. Polym. 181 (2018) 43–55, https://doi.org/10.1016/j.carbpol.2017.10.051.

[30] R.M.A. Daoub, A.H. Elmubarak, M. Misran, E.A. Hassan, M.E. Osman, Characterization and functional properties of some natural Acacia gums, J. Saudi Soc. Agric. Sci. 17 (2018) 241–249, https://doi.org/10.1016/j.jssas.2016.05.002.

[31] A. Mitsuzuka, A. Fujii, T. Ebata, N. Mikami, Infrared spectroscopy of OH stretching vibrations of hydrogen-bonded tropolone-(H_2O)n (n=1-3) and tropolone-(CH_3OH)n (n=1 and 2) clusters, J. Chem. Phys. 105 (1996) 2618–2627, https://doi.org/10.1063/1.472126.

[32] E. Wiercigroch, E. Szafraniec, K. Czamara, M.Z. Pacia, K. Majzner, K. Kochan, A. Kaczor, M. Baranska, K. Malek, Raman and infrared spectroscopy of carbohydrates: a review, Spectrochim. Acta Part A Mol. Biomol. Spectrosc. 185 (2017) 317–335, https://doi.org/10.1016/j.saa.2017.05.045.

[33] F. Long, Z. Chen, K. Han, L. Zhang, W. Zhuang, Differentiation between enamines and tautomerizable imines oxidation reaction mechanism using electron-vibration-vibration two dimensional infrared spectroscopy, Molecules 24 (2019)https://doi.org/10.3390/molecules24050869.

[34] E. Mellado-Mojica, N.P. Seeram, M.G. López, Comparative analysis of maple syrups and natural sweeteners: carbohydrates composition and classification (differentiation) by HPAEC-PAD and FTIR spectroscopy-chemometrics, J. Food Compos. Anal. 52 (2016) 1–8, https://doi.org/10.1016/j.jfca.2016.07.001.

[35] P. Janoš, T. Hladík, M. Kormunda, J. Ederer, M. Šťastný, Thermal treatment of cerium oxide and its properties: adsorption ability versus degradation efficiency, Adv. Mater. Sci. Eng. 2014 (2014)https://doi.org/10.1155/2014/706041.

[36] C.G. Mothé, M.A. Rao, Thermal behavior of gum arabic in comparison with cashew gum, Thermochim. Acta 357–358 (2000) 9–13, https://doi.org/10.1016/S0040-6031(00)00358-0.
[37] Y. Morozov, L.M. Calado, R.A. Shakoor, R. Raj, R. Kahraman, M.G. Taryba, M.F. Montemor, Epoxy coatings modified with a new cerium phosphate inhibitor for smart corrosion protection of steel, Corros. Sci. 159 (2019) 108128, https://doi.org/10.1016/j.corsci.2019.108128.
[38] C. Shen, V. Alvarez, J.D.B. Koenig, J.L. Luo, Gum Arabic as corrosion inhibitor in the oil industry: experimental and theoretical studies, Corros. Eng. Sci. Technol. 54 (2019) 444–454, https://doi.org/10.1080/1478422X.2019.1613780.
[39] F. Zhang, P. Ju, M. Pan, D. Zhang, Y. Huang, G. Li, X. Li, Self-healing mechanisms in smart protective coatings: a review, Corros. Sci. 144 (2018) 74–88, https://doi.org/10.1016/j.corsci.2018.08.005.
[40] A.S. Patel, V.A. Panchal, G.V. Mudaliar, N.K. Shah, Impedance spectroscopic study of corrosion inhibition of Al-Pure by organic Schiff base in hydrochloric acid, J. Saudi Chem. Soc. 17 (2013) 53–59, https://doi.org/10.1016/j.jscs.2011.06.003.
[41] H. Vakili, B. Ramezanzadeh, R. Amini, The corrosion performance and adhesion properties of the epoxy coating applied on the steel substrates treated by cerium-based conversion coatings, Corros. Sci. 94 (2015) 466–475, https://doi.org/10.1016/j.corsci.2015.02.028.
[42] G. Bahlakeh, B. Ramezanzadeh, M.R. Saeb, H. Terryn, M. Ghaffari, Corrosion Protection Properties and Interfacial Adhesion Mechanism of an Epoxy/Polyamide Coating Applied on the Steel Surface Decorated with Cerium Oxide Nanofilm: Complementary Experimental, Molecular Dynamics (MD) and First Principle Quantum Mechanics, Elsevier B.V., 2017. doi:https://doi.org/10.1016/j.apsusc.2017.05.070.
[43] I.O. Arukalam, E.Y. Ishidi, H.C. Obasi, I.O. Madu, O.E. Ezeani, M.M. Owen, Exploitation of natural gum exudates as green fillers in self-healing corrosion-resistant epoxy coatings, J. Polym. Res. 27 (2020)https://doi.org/10.1007/s10965-020-02055-y.
[44] K. Azzaoui, E. Mejdoubi, S. Jodeh, A. Lamhamdi, E. Rodriguez-Castellón, M. Algarra, A. Zarrouk, A. Errich, R. Salghi, H. Lgaz, Eco friendly green inhibitor Gum Arabic (GA) for the corrosion control of mild steel in hydrochloric acid medium, Corros. Sci. 129 (2017) 70–81, https://doi.org/10.1016/j.corsci.2017.09.027.
[45] F.C. Walsh, C. Ponce de León, C. Kerr, S. Court, B.D. Barker, Electrochemical characterisation of the porosity and corrosion resistance of electrochemically deposited metal coatings, Surf. Coatings Technol. 202 (2008) 5092–5102, https://doi.org/10.1016/j.surfcoat.2008.05.008.
[46] A.B. Radwan, R.A. Shakoor, Aluminum nitride (AlN) reinforced electrodeposited Ni–B nanocomposite coatings, Ceram. Int. (2020) 0–1. doi:https://doi.org/10.1016/j.ceramint.2019.12.261.
[47] A. Biswas, P. Mourya, D. Mondal, S. Pal, G. Udayabhanu, Grafting effect of gum acacia on mild steel corrosion in acidic medium: gravimetric and electrochemical study, J. Mol. Liq. 251 (2018) 470–479, https://doi.org/10.1016/j.molliq.2017.12.087.
[48] E.E. Oguzie, Y. Li, F.H. Wang, Effect of 2-amino-3-mercaptopropanoic acid (cysteine) on the corrosion behaviour of low carbon steel in sulphuric acid, Electrochim. Acta 53 (2007) 909–914, https://doi.org/10.1016/j.electacta.2007.07.076.
[49] S.A. Umoren, O. Ogbobe, I.O. Igwe, E.E. Ebenso, Inhibition of mild steel corrosion in acidic medium using synthetic and naturally occurring polymers and synergistic halide additives, Corros. Sci. 50 (2008) 1998–2006, https://doi.org/10.1016/j.corsci.2008.04.015.
[50] P. Roy, P. Karfa, U. Adhikari, D. Sukul, Corrosion inhibition of mild steel in acidic medium by polyacrylamide grafted Guar gum with various grafting percentage: effect of intramolecular synergism, Corros. Sci. 88 (2014) 246–253, https://doi.org/10.1016/j.corsci.2014.07.039.
[51] J. Buchweishaija, G.S. Mhinzi, Natural products as a source of environmentally friendly corrosion inhibitors: The case of gum exudate from *Acacia seyal* var. seyal, Port. Electrochim. Acta 26 (2008) 257–265, https://doi.org/10.4152/pea.2008032257.